Eur. Phys. J. Plus (2026) 141:929
https://doi.org/10.1140/epjp/s13360-026-08021-9

THE EUROPEAN PHYSICAL JOURNAL PLUS

Regular Article

Closed-form resistance and self-inductance of transformer-induced eddy currents in long plates

Maria Mauraza[a], **María Jesús Elejabarrieta**[b], **Fernando Cortés**[c]

Department of Mechanics, Design and Industrial Management, University of Deusto, Avda. de Las Universidades 24, 48007 Bilbao, Spain

Received: 30 March 2026 / Accepted: 25 June 2026

Abstract Eddy currents play a key role in a wide range of applications, including induction heating, non-destructive testing, braking, and non-contact damping. The determination of their equivalent electrical parameters, particularly resistance and self-inductance, is essential for physical interpretation and for the validation of numerical models, yet explicit closed-form formulations remain scarce. In this work, closed-form expressions are derived for the resistance and self-inductance associated with transformer-induced eddy currents in conducting plates with large aspect ratios. The analytical formulation enables the evaluation of the induced magnetic field, magnetic flux, and Joule losses, leading to compact expressions for the equivalent electrical parameters and a consistent RL circuit representation of the system. The proposed expressions provide an analytical benchmark for the validation and interpretation of numerical models of transformer-induced eddy currents in long conducting plates. The results are compared with existing analytical approximations obtained under more restrictive assumptions, demonstrating consistency while providing a physically consistent analytical description within the assumptions of dominant longitudinal currents and large aspect ratios.

1 Introduction

When a conductive plate is subjected to a time-varying magnetic field, eddy currents are induced. These currents are widely used in applications such as braking systems [1], non-contact damping [2], metal separation [3], and sensors [4] and also play a significant role in energy dissipation in transformers [5] and electrical machines [6]. In complex geometries, their effects are typically analysed using numerical methods [7], whereas analytical solutions remain comparatively scarce. Nevertheless, simple closed-form expressions, although less common, provide valuable physical insight and enable rapid validation of computational models.

Analytical solutions for the associated electrical parameters in several idealised configurations have been reported in the literature, including the studies by Bialek [8], Siakavellas [9], and Ekman [10, 11]. Bialek assumes currents to be uniformly distributed across the width of the plate, whereas Siakavellas models them as concentric rectangular loops. Ekman proposes an analytical approximation for the equivalent electrical parameters of thin rectangular wires.

However, explicit closed-form results for plates with a dominant dimension remain scarce. In this work, closed-form expressions for the resistance and self-inductance associated with transformer-induced eddy currents in long conducting plates are derived from an analytical current distribution based on less restrictive assumptions. The formulation enables the analytical evaluation of the induced magnetic field and magnetic flux, leading to a consistent equivalent RL representation of the system. The obtained expressions are compared with previously reported simplified analytical models, highlighting their differences and showing that the present formulation, based on less restrictive assumptions, provides a more consistent analytical description within the assumptions of long thin conducting plates.

2 System description

In this study, a thin plate of conductivity σ, length L_x, width L_y, and thickness L_z is considered, with $L_y < L_x$ and $L_z \ll L_x$. The plate lies in the x–y plane, where the x-axis corresponds to the longitudinal direction of length L_x, the y-axis to the transverse direction of L_y, and the z-axis is normal to the plate. The coordinate system is defined such that the origin is located at the centre of the plate. A uniform time-harmonic magnetic field with flux density amplitude B and angular frequency ω is applied in the z-direction.

[a] e-mail: mauraza.maria@deusto.es
[b] e-mail: maria.elejabarrieta@deusto.es
[c] e-mail: fernando.cortes@deusto.es (corresponding author)

Published online: 12 August 2026

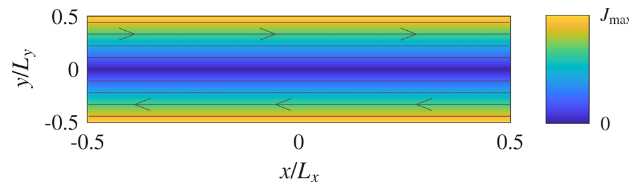

Fig. 1 Dominant longitudinal eddy-current distribution induced by transformer excitation in a long conducting plate under the large-aspect-ratio approximation

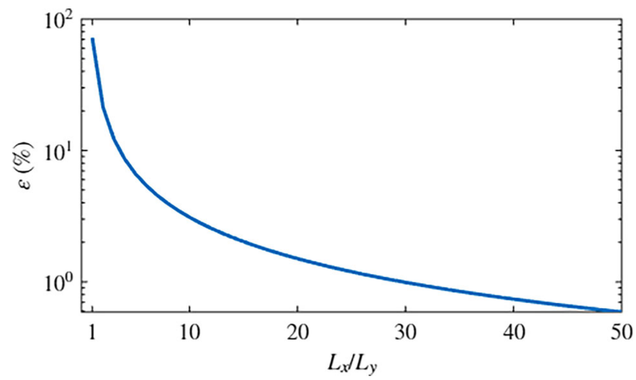

Fig. 2 Global quadratic error between numerical and modelled current distributions for ratios 1 through 50

The analysis is carried out under the magneto–quasi-static approximation, assuming that the electromagnetic wavelength associated with the applied magnetic field is much larger than the plate dimensions [12].

The interaction between the magnetic field and the conductive plate induces eddy currents. Their spatial distribution is assumed to be predominantly longitudinal along the x-direction, neglecting the end-region recirculation required to close the eddy-current paths, as illustrated in Fig. 1. Additionally, since the plate is assumed to be sufficiently thin, the current distribution is considered uniform across the thickness. Then, the current density distribution amplitude, as detailed in [12], can be written as

$$\mathbf{J}(y) = J_x(y)\hat{\mathbf{x}} = J_{\max}\frac{2y}{L_y}\hat{\mathbf{x}}, \tag{1}$$

where $J_{\max} = \omega\sigma B L_y \big/ 2$.

Boundary effects are known to become less significant as the length-to-width ratio increases, as illustrated by the current distributions shown in Fig. 6 of Appendix A, obtained using the numerical method presented in [13]. These results, including ratios that do not satisfy $L_y < L_x$, show that, as the aspect ratio increases and satisfies $L_y < L_x$, the current paths progressively approach the theoretical behaviour predicted by Eq. (1) and depicted in Fig. 1. In particular, the recirculation required to close the eddy-current paths becomes confined to the shortest plate edges, while the dominant current component becomes predominantly longitudinal.

The colour bars in Fig. 6 indicate the local current density normalised with respect to the maximum theoretical longitudinal current density $J_{\max}$ predicted by Eq. (1). The maximum values in the colour bars are the maximum values of J_x, which occur at $(x, y) = (0, \pm L_y/2)$. It can be observed that, from an aspect ratio of 5 onwards, the current distribution predicted by Eq. (1) closely matches the numerical results.

To further evaluate the validity of the proposed approximation, a global relative quadratic error between the numerically evaluated current distributions $\mathbf{J}_{\text{num}}$ and the analytical distribution $\mathbf{J}_{\text{model}}$ given by Eq. (1) is calculated. Since an exact analytical solution $\mathbf{J}_{\text{exact}}$ is not available, the numerical solution obtained using the finite-difference model is taken as the reference distribution. The error ε is then defined as

$$\varepsilon = \frac{\int_A |\mathbf{J}_{\text{exact}}(x, y) - \mathbf{J}_{\text{model}}(x, y)|^2 \mathrm{d}A}{\int_A |\mathbf{J}_{\text{exact}}(x, y)|^2 \mathrm{d}A} \approx \frac{\sum_{i=1}^{n} \left|\mathbf{J}_{\text{num},i} - \mathbf{J}_{\text{model}}(x_i, y_i)\right|^2}{\sum_{i=1}^{n} \left|\mathbf{J}_{\text{num},i}\right|^2}, \tag{2}$$

where $(x_i,\ y_i)$ represent the coordinates of the ith node, and n is the total number of nodes of the numerical model. Figure 2 illustrates this error for ratios 1 through 50. From these results, it can be pointed out that, for ratio 10, the error is 3.1%, for ratio 20 it is 1.5% and for ratio 30, 0.99%.

It can be concluded that, for ratios higher than 10, the model provides a good approximation of the expected results and therefore the present analysis assumes $L_x/L_y \geq 10$.

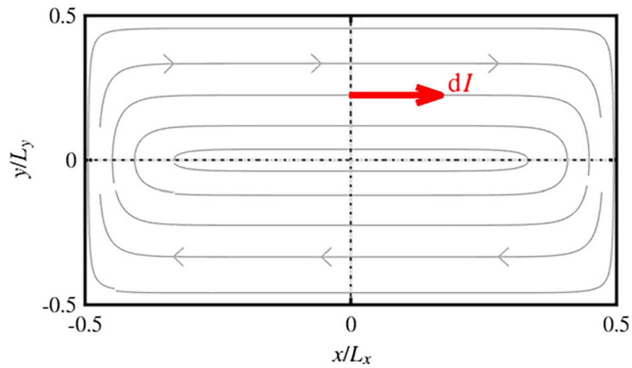

Fig. 3 Interpretation of the distributed eddy-current system as a continuum of elementary closed current loops and their associated differential circulating current dI

3 Closed-form expressions for equivalent resistance and self-inductance

In this section, closed-form expressions for the equivalent resistance and self-inductance are derived. The formulation is based on the analytical evaluation for the power amplitude of Joule's losses, the total circulating current amplitude and the induced magnetic field and magnetic flux, with the equivalent resistance and inductance evaluation approach carried out as proposed in [9].

3.1 Equivalent electrical resistance

The equivalent electrical resistance R of the plate can be obtained from Joule's law,

$$P_\mathrm{J} = I^2 R, \tag{3}$$

where P_J denotes the amplitude of the instantaneous Joule power dissipated in the conductor and I represents the amplitude of the total circulating current. Although the conducting plate is not a discrete multi-turn coil, the induced eddy currents form circulating paths continuously distributed over the plate surface. These current paths can be interpreted as a continuum of elementary planar current loops of different sizes lying on the same plane, as illustrated in Fig. 3.

For the elementary loop located at the transverse coordinate y, the associated differential circulating current dI, as pictured for one of the loops in Fig. 3, is defined from the longitudinal current density crossing the central section $x = 0$, namely

$$\mathrm{d}I = J_x(0, y)\,\mathrm{d}y\,\mathrm{d}z. \tag{4}$$

The resulting equivalent circulating current follows the distributed closed-loop interpretation adopted in [9] and can therefore be consistently used in the present model while satisfying charge conservation for the dominant longitudinal current component. Consequently, the total equivalent circulating current is obtained by integrating these elementary contributions over half of the plate width, yielding

$$I = \int_{-L_z/2}^{L_z/2} \int_0^{L_y/2} J_x(y)\,\mathrm{d}y\,\mathrm{d}z = \frac{J_{\max} L_y L_z}{4}. \tag{5}$$

On the other hand, Joule's losses can be derived from the current density vector field $\mathbf{J}$ from the local form of Joule's law, which gives

$$P_\mathrm{J} = \int_{-L_z/2}^{L_z/2} \int_{-L_y/2}^{L_y/2} \int_{-L_x/2}^{L_x/2} \frac{|\mathbf{J}(x, y, z)|^2}{\sigma} \mathrm{d}x\,\mathrm{d}y\,\mathrm{d}z = \frac{J_{\max}^2 L_x L_y L_z}{3\sigma} \tag{6}$$

Finally, substituting these expressions into Eq. (3), the equivalent resistance R_p proposed in this paper results in

$$R_\mathrm{p} = \frac{16}{3\sigma L_z} \frac{L_x}{L_y}. \tag{7}$$

It can be noted that this resistance is proportional to the aspect ratio of the plate L_x/L_y and inversely proportional to the thickness of the plate L_z.

3.2 Equivalent self-inductance

The equivalent electrical self-inductance L of the plate can be obtained from the proportionality between the magnetic flux linkage and the equivalent circulating current. Since the induced currents are continuously distributed over the conducting plate rather than flowing through a discrete multi-turn circuit, the magnetic flux linkage is here defined as the total magnetic flux associated with the distributed eddy-current loops defining the equivalent circulating current. Under this interpretation,

$$\Phi = LI, \tag{8}$$

where Φ denotes the magnetic flux linked with the circulating currents and is obtained from the induced magnetic field $B_z(x, y)$. Consequently, the inductance derived in this work should be interpreted as an equivalent inductance associated with the RL representation of the distributed eddy-current system. Accordingly, the formulation is also consistent with the classical magnetic-energy relation

$$W_\mathrm{m} = \frac{1}{2}\Phi I = \frac{1}{2}LI^2. \tag{9}$$

To calculate the induced magnetic field, the plate surface is modelled as a set of parallel differential filaments with currents dI in x-direction, which, for the wire located at the y'-position results in

$$\mathrm{d}I(y') = J_x(y')L_z\mathrm{d}y'. \tag{10}$$

The differential magnetic field B_z induced at a point with coordinates (x,y) can then be expressed as

$$\mathrm{d}B_z(x, y, y') = \frac{\mu_0}{4\pi}\left[\frac{L_x/2 - x}{(y - y')\sqrt{(x - L_x/2)^2 + (y - y')^2}} + \frac{L_x/2 + x}{(y - y')\sqrt{(x + L_x/2)^2 + (y - y')^2}}\right]\mathrm{d}I(y'). \tag{11}$$

To derive a closed-form expression for the magnetic field over the plate from Eq. (11), the integral is evaluated in the Cauchy principal value sense to handle the singularity of the kernel

$$B_z(x, y) = \frac{J_{\max}\mu_0 L_z}{2\pi L_y}\mathrm{p.v.}\int_{-L_y/2}^{L_y/2} y'\left(\frac{L_x/2 - x}{(y - y')\sqrt{(x - L_x/2)^2 + (y - y')^2}} + \frac{L_x/2 + x}{(y - y')\sqrt{(x + L_x/2)^2 + (y - y')^2}}\right)\mathrm{d}y'. \tag{12}$$

The detailed integration process can be found in Appendix B and yields

$$\begin{aligned}
B_z(x, y) = &\frac{\mu_0 J_{\max} L_z}{2\pi L_y}\Bigg\{-\left(\frac{L_x}{2} + x\right)\ln\left[\frac{L_y}{2} + y + \sqrt{\left(\frac{L_x}{2} + x\right)^2 + \left(\frac{L_y}{2} + y\right)^2}\right] \\
&+ \left(\frac{L_x}{2} + x\right)\ln\left[-\left(\frac{L_y}{2} - y\right) + \sqrt{\left(\frac{L_x}{2} + x\right)^2 + \left(\frac{L_y}{2} - y\right)^2}\right] \\
&- \left(\frac{L_x}{2} - x\right)\ln\left[\frac{L_y}{2} + y + \sqrt{\left(\frac{L_x}{2} - x\right)^2 + \left(\frac{L_y}{2} + y\right)^2}\right] \\
&+ \left(\frac{L_x}{2} - x\right)\ln\left[-\left(\frac{L_y}{2} - y\right) + \sqrt{\left(\frac{L_x}{2} - x\right)^2 + \left(\frac{L_y}{2} - y\right)^2}\right] \\
&- y\left[2\ln\left(\frac{L_y}{2} - y\right) - 2\ln\left(\frac{L_y}{2} + y\right)\right] \\
&+ y\ln\left[\frac{L_x}{2} + x + \sqrt{\left(\frac{L_x}{2} + x\right)^2 + \left(\frac{L_y}{2} - y\right)^2}\right] \\
&- y\ln\left[\frac{L_x}{2} + x + \sqrt{\left(\frac{L_x}{2} + x\right)^2 + \left(\frac{L_y}{2} + y\right)^2}\right] \\
&+ y\ln\left[\frac{L_x}{2} - x + \sqrt{\left(\frac{L_x}{2} - x\right)^2 + \left(\frac{L_y}{2} - y\right)^2}\right] - y\ln\left[\frac{L_x}{2} - x + \sqrt{\left(\frac{L_x}{2} - x\right)^2 + \left(\frac{L_y}{2} + y\right)^2}\right]\Bigg\}.
\end{aligned} \tag{13}$$

By analysing Eq. (13), several properties of the induced magnetic field can be identified. First, the field exhibits symmetry with respect to both the x- and y-axes. Second, it should be noted that the induced magnetic field tends to infinity when $y \to \pm L_y/2$, which is a consequence of the line-current approximation adopted in the formulation.

Additionally, when $x = L_x/2$, Eq. (13) becomes indeterminate due to terms of the form $0{\cdot}\infty$. However, evaluating the limit as $x \to L_x/2$ yields a finite expression given by

Fig. 4 Magnetic field generated over a quarter of the plate

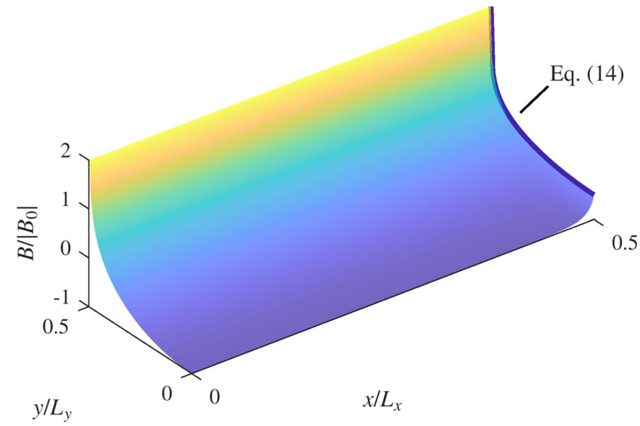

$$\lim_{x\to L_x/2^-} B_z(x,y) = \frac{\mu_0 J_{\max} L_z}{2\pi L_y}\Bigg\{ L_x \ln\left[-\left(\frac{L_y}{2}-y\right)+\sqrt{L_x^2+\left(\frac{L_y}{2}-y\right)^2}\right] - L_x \ln\left[\frac{L_y}{2}+y+\sqrt{L_x^2+\left(\frac{L_y}{2}+y\right)^2}\right] - y\ln\left(\frac{L_y}{2}-y\right)+y\ln\left(\frac{L_y}{2}+y\right) - y\ln\left[L_x+\sqrt{L_x^2+\left(\frac{L_y}{2}+y\right)^2}\right] + y\ln\left[L_x+\sqrt{L_x^2+\left(\frac{L_y}{2}-y\right)^2}\right]\Bigg\}. \tag{14}$$

Figure 4 shows the magnetic field density at a quarter of the plate, normalised to the absolute value of the induced field B_0 at its centre point (0,0), which results in

$$B_0 = -\frac{\mu_0 J_{\max} L_x L_z}{\pi L_y}\ln\left(\frac{L_y+\sqrt{L_x^2+L_y^2}}{L_x}\right). \tag{15}$$

Note that, for visualisation purposes, the magnetic field shown in Fig. 4 is truncated at 2 to better illustrate the spatial distribution across the plate. It represents its bowl-like shape with a minimum value at its centre. Equation (14) is also plotted in Fig. 4 in dark blue along the right-hand edge of the field.

From Eq. (13), the induced magnetic flux over the plate can be obtained by integrating as

$$\Phi = 4\int_0^{L_x/2}\int_0^{L_y/2} B_z(x,y)\,\mathrm{d}y\,\mathrm{d}x. \tag{16}$$

Equation (16) is an improper integral, as $B_z(x,\ y)$ tends to infinity along an edge of the plate. However, its result converges to a finite expression, yielding

$$\Phi = \frac{\mu_0 J_{\max} L_z}{\pi L_y}\left[\frac{L_x^3}{3}-\frac{L_y^3}{6}-\frac{2L_x^2-L_y^2}{6}\sqrt{L_x^2+L_y^2}+\frac{L_x^2 L_y}{2}\ln\left(\frac{L_y+\sqrt{L_x^2+L_y^2}}{L_x}\right)\right]. \tag{17}$$

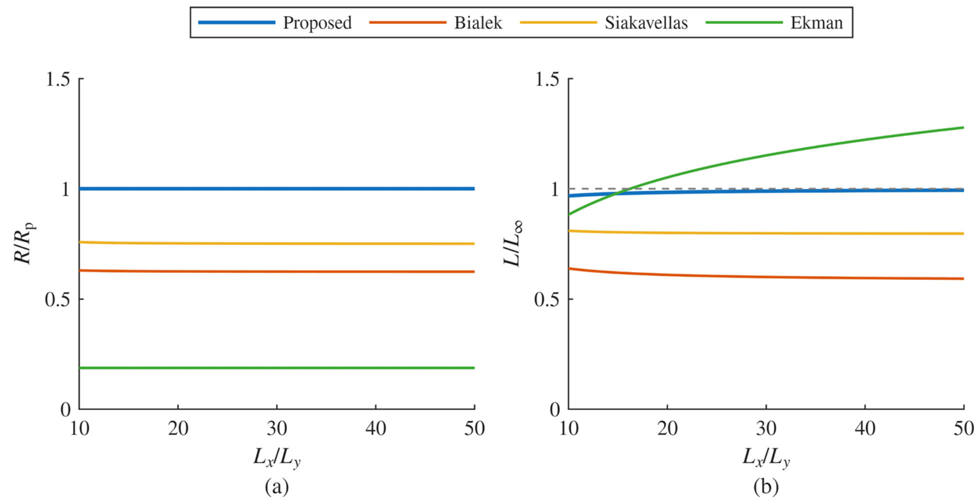

Fig. 5 Comparison for the electrical properties between existing models and presented expressions: **a** resistance normalised to R_p and **b** self-inductance normalised to L_∞

From Eq. (8), the equivalent inductance presented in this paper L_p results in

$$L_\mathrm{p} = \frac{4\mu_0}{\pi L_y^2}\left[\frac{L_x^3}{3} - \frac{L_y^3}{6} - \frac{2L_x^2 - L_y^2}{6}\sqrt{L_x^2 + L_y^2} + \frac{L_x^2 L_y}{2}\ln\left(\frac{L_y + \sqrt{L_x^2 + L_y^2}}{L_x}\right)\right]. \tag{18}$$

This expression can alternatively be rewritten as a function of the ratio L_x/L_y, after expressing the logarithmic term as an inverse hyperbolic sine, which yields

$$L_\mathrm{p} = \frac{4\mu_0 L_x}{\pi}\left[\frac{L_x^2}{3L_y^2} - \frac{L_y}{6L_x} - \left(\frac{L_x^2}{3L_y^2} - \frac{1}{6}\right)\sqrt{1 + \frac{L_y^2}{L_x^2}} + \frac{L_x}{2L_y}\sinh^{-1}\frac{L_y}{L_x}\right]. \tag{19}$$

When $L_x \to \infty$, neglecting higher order terms, the following approximations can be made:

$$\sqrt{1 + \frac{L_y^2}{L_x^2}} \approx 1 + \frac{1}{2}\frac{L_y^2}{L_x^2} \tag{20}$$

and

$$\sinh^{-1}\frac{L_y}{L_x} \approx \frac{L_y}{L_x} \tag{21}$$

Substituting Eqs. (20) and (21) into Eq. (19) while neglecting terms proportional to L_y/L_x and proportional to L_y^2/L_x^2, yields

$$L_\infty = \frac{2\mu_0}{\pi}L_x, \tag{22}$$

which satisfies

$$\lim_{L_x\to\infty}\frac{L_\mathrm{p}}{L_\infty} = 1. \tag{23}$$

This result confirms the expected asymptotic behaviour of the inductance reported by Bialek [8] and Siakavellas [14], and coincides with the expression that would be obtained for infinitely long current filaments in Eq. (11).

4 Comparison

In this section, the expressions for the equivalent resistance and self-inductance derived in this work are compared with other analytical models reported in the literature as a function of the length-to-width ratio, as shown in Fig. 5. Since the proposed model is derived under the assumption $L_x/L_y \geq 10$, the comparison is restricted to this range. The compared analytical models are detailed in Appendix C, as well as their asymptotic values.

On the one hand, the normalised equivalent resistances R/R_{p} are shown in Fig. 5a, where the proposed resistance R_{p} is given by Eq. (7). While the models presented by Bialek and Siakavellas decrease with the ratio and approach asymptotic values for the illustrated range, the proposed resistance and that reported by Ekman remain constant. Note that those models are approximately $R_{\text{B},\infty}/R_{\text{p}} = 0.62$, $R_{\text{S},\infty}/R_{\text{p}} = 0.75$, and $R_{\text{E}}/R_{\text{p}} = 0.19$, respectively, which can be derived from the expressions in Appendix C.

On the other hand, Fig. 5b shows the normalised equivalent self-inductances L/L_∞, as well as a dotted line representing the asymptotic expression for L_∞. The expressions reported by Bialek and Siakavellas approach asymptotic values for the considered ratios, leading to an underestimation of the equivalent self-inductance, specifically, the asymptotic relationships are $L_{\text{B},\infty}/L_\infty = 0.58$ and $L_{\text{S},\infty}/L_\infty = 0.80$. In contrast, the model proposed by Ekman exhibits a logarithmic dependence and increases with the aspect ratio. These relationships are also derived from the asymptotic expressions in Appendix C.

Finally, it can be pointed out that, for ratio 10, the normalised value of the presented self-inductance is 0.97, which indicates that, for practical use, the asymptotic expression from Eq. (22) can be used without a significant loss of accuracy.

5 Conclusions

In this work, closed-form expressions for the equivalent resistance and self-inductance associated with transformer-induced eddy currents in long conducting plates have been derived. These expressions provide a simple analytical description of the electrical behaviour of plates with large length-to-width ratios.

The proposed formulation allows the electromagnetic problem considered to be represented by an equivalent RL electrical circuit, which greatly simplifies the interpretation of the underlying physical phenomena. In addition, the obtained expressions provide a convenient analytical benchmark for validating numerical methods commonly used to analyse transformer-induced currents in conducting plates within the assumptions of dominant longitudinal currents and large aspect ratios.

Acknowledgements This study has received financial support from the Spanish Ministry of Science, Innovation and Universities through the project PID2024-158168OB-I00.

Funding Open Access funding provided thanks to the CRUE-CSIC agreement with Springer Nature. Ministerio de Ciencia, Innovación y Universidades, PID2024-158168OB-I00.

Data availability statement The datasets generated during and/or analyzed during the current study are available from the corresponding author on reasonable request.

Declarations

Conflict of interest The authors declare no conflict of interest.

Appendix A. Current maps for different aspect ratios

Current maps for transformer-induced eddy currents in rectangular conducting plates with length-to-width ratios $L_x/L_y = 1, 2, 5,$ 10, and 20 are shown in Fig. 6. These maps were obtained using the numerical method presented in [13] and illustrate the progressive dominance of the longitudinal current component as the aspect ratio increases. The current maps are normalised with respect to the maximum theoretical longitudinal current density J_{max} predicted in Eq. (1). For visualization purposes, the geometrical scales of the plates shown in Fig. 6 are not represented proportionally to their actual dimensions. Consequently, the displayed geometries do not preserve the actual aspect-ratio scaling.

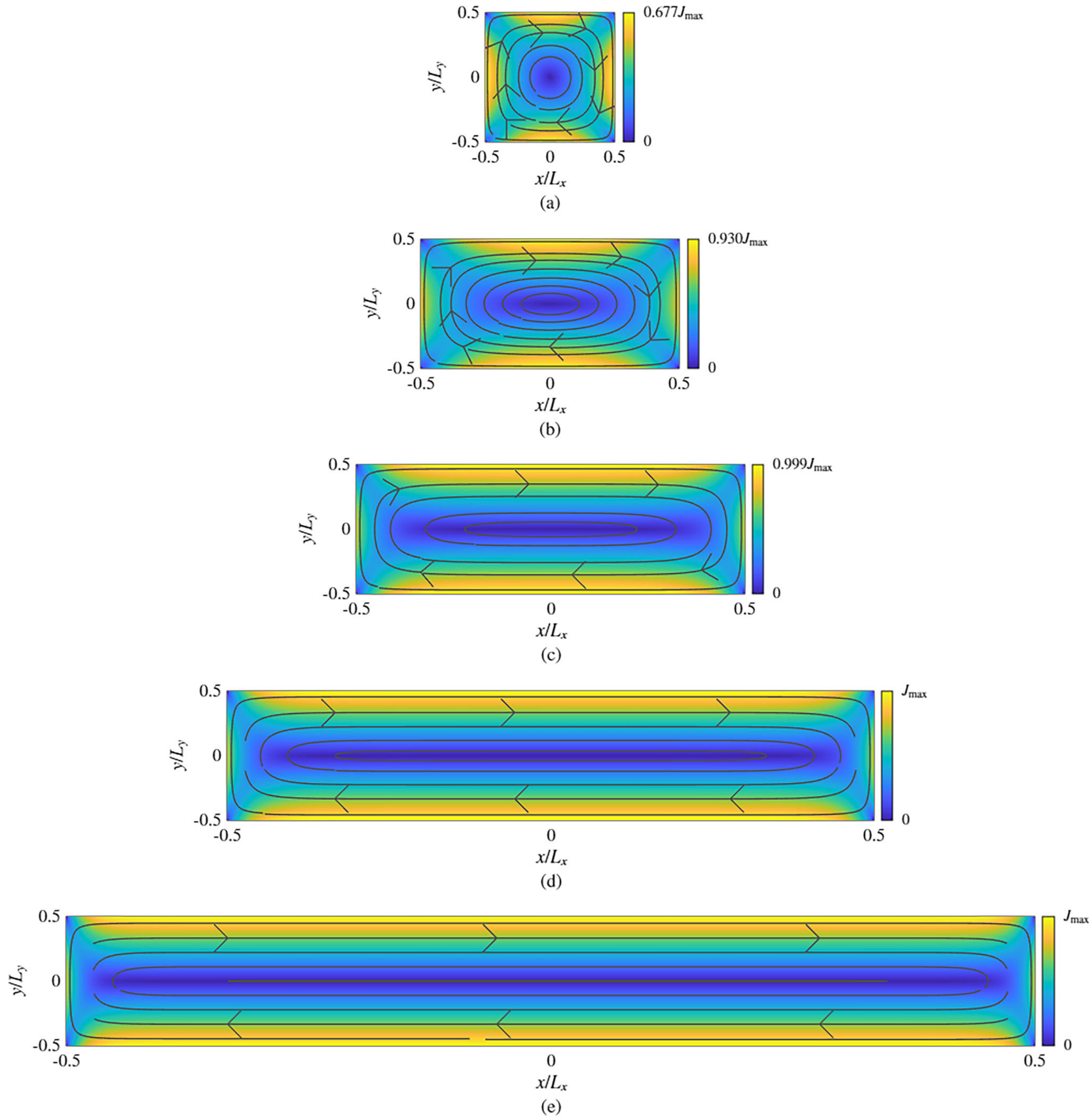

Fig. 6 Normalised current maps for transformer-induced eddy currents in rectangular conducting plates for different aspect ratios L_x/L_y: **a** 1, **b** 2, **c** 5, **d** 10, and **e** 20

Appendix B. Detailed integration for induced magnetic field and induced magnetic flux

In this appendix, the integration of the differential singular kernel in Eq. (12) is detailed, to obtain induced magnetic field and magnetic flux. Firstly, a variable change is performed in Eq. (12), where $u = y - y'$ and $y' = y - u$, which yields

$$B_z(x, y) = \frac{J_{\max}\mu_0 L_z}{2\pi L_y} p.v. \int_{y-L_y/2}^{y+L_y/2} \left(\frac{y(L_x/2 - x)}{u\sqrt{u^2 + (x - L_x/2)^2}} - \frac{(L_x/2 - x)}{\sqrt{u^2 + (x - L_x/2)^2}} + \frac{y(L_x/2 + x)}{u\sqrt{u^2 + (x + L_x/2)^2}} - \frac{(L_x/2 + x)}{\sqrt{u^2 + (x + L_x/2)^2}} \right) \mathrm{d}u \tag{24}$$

The separate addends have known primitives, which makes the integration process in the Cauchy principal value sense easier. Its result is precisely Eq. (13). As mentioned in the main body of this work, this expression tends to infinity when $y \to \pm L_y/2$. However, integrating over the plate surface results in a finite expression.

To obtain a closed-form finite expression for the induced magnetic flux, the induced magnetic field is first integrated along half the plate width. To ease the integration process, Eq. (13) is separated into the terms containing $\pm\big(y + L_y/2\big)$ and those containing $\pm\big(y - L_y/2\big)$. The latter are evaluated in the Cauchy principal value sense. Integration along half the plate width then yields

$$\begin{aligned}
\mathrm{d}\Phi(x) = \frac{J_{\max}\mu_0 L_z}{2\pi L_y}\Bigg[& \frac{1}{2}\left(\frac{L_x}{2}+x\right)\sqrt{\left(\frac{L_x}{2}+x\right)^2+L_y^2} - \frac{1}{2}\left(\frac{L_x}{2}-x\right)^2 + \frac{1}{2}\left(\frac{L_x}{2}-x\right)\sqrt{\left(\frac{L_x}{2}-x\right)^2+L_y^2} \\
& - \frac{1}{2}\left(\frac{L_x}{2}+x\right)^2 - \frac{L_y}{2}\ln\left(L_y+\sqrt{\left(\frac{L_x}{2}-x\right)^2+L_y^2}\right)\left(\frac{L_x}{2}-x\right) \\
& + \frac{L_y}{2}\ln\left(\sqrt{\left(\frac{L_x}{2}+x\right)^2+\frac{L_y^2}{4}}-\frac{L_y}{2}\right)\left(\frac{L_x}{2}+x\right) \\
& + \frac{L_y}{2}\ln\left(\frac{L_y}{2}+\sqrt{\left(\frac{L_x}{2}+x\right)^2+\frac{L_y^2}{4}}\right)\left(\frac{L_x}{2}+x\right) \\
& - \frac{L_y}{2}\ln\left(L_y+\sqrt{\left(\frac{L_x}{2}+x\right)^2+L_y^2}\right)\left(\frac{L_x}{2}+x\right) \\
& \frac{-L_y}{2}\ln\left(\frac{L_x}{2}-x\right)\left(\frac{L_x}{2}-x\right) \\
& + \frac{L_y}{2}\ln\left(\sqrt{\left(\frac{L_x}{2}-x\right)^2+\frac{L_y^2}{4}}-\frac{L_y}{2}\right)\left(\frac{L_x}{2}-x\right) \\
& + \frac{L_y}{2}\ln\left(\frac{L_y}{2}+\sqrt{\left(\frac{L_x}{2}-x\right)^2+\frac{L_y^2}{4}}\right)\left(\frac{L_x}{2}-x\right) - \frac{L_y}{2}\ln\left(\frac{L_x}{2}+x\right)\left(\frac{L_x}{2}+x\right)\Bigg]
\end{aligned} \tag{25}$$

Equation (25) has two $\ln\infty$ terms when evaluated at $x \to \pm L_x/2$. To obtain a finite closed-form expression for the flux, $\mathrm{d}\Phi(x)$ is evaluated in the principal value sense to integrate along half the plates length, yielding the expression in Eq. (17). The use of the Cauchy principal value provides a finite and well-defined closed-form result for the magnetic flux despite the logarithmic singularity of the magnetic field at the plate edges.

Appendix C. Analytical expressions used in the comparison

This appendix summarises the analytical expressions employed to generate the reference curves shown in Fig. 5. The formulations corresponding to the models proposed by Bialek, Siakavellas, and Ekman are listed below for both the equivalent resistance and the equivalent self-inductance. These formulations are based on the assumptions of uniform current distribution, rectangular current loops, and thin-wire approximation, respectively. The notation follows that introduced in the main text. In particular, L_x, L_y and L_z denote the plate length, width, and thickness, respectively, while σ and μ_0 represent the electrical conductivity and vacuum permeability.

Equivalent resistance

Bialek [8]:

$$R_{\mathrm{B}} = 1.665\frac{2}{\sigma L_z}\left(\frac{L_x^2+L_y^2}{L_x L_y}\right). \tag{26}$$

Siakavellas [9]:

$$R_{\mathrm{S}} = \frac{4}{\sigma L_z}\left(\frac{L_x^2+L_y^2}{L_x L_y}\right). \tag{27}$$

Ekman [11]:

$$R_{\mathrm{E}} = \frac{L_x}{\sigma L_y L_z}. \tag{28}$$

Equivalent self-inductance

Bialek [8]:

$$L_{\mathrm{B}} = 1.665 \frac{2\mu_0}{9} (L_x + L_y). \tag{29}$$

Siakavellas [9]:

$$\begin{aligned} L_S = &\frac{2\mu}{3\pi} \left\{ L_x \left[1 + \ln\left(\frac{L_x + \sqrt{L_x^2 + L_y^2}}{L_y} \right) \right] + L_y \left[1 + \ln\left(\frac{L_y + \sqrt{L_x^2 + L_y^2}}{L_x} \right) \right] \right. \\ &\left. + \frac{L_x^2 - L_y^2}{\sqrt{L_x^2 + L_y^2}} \ln\left[\frac{L_y\left(L_x + \sqrt{L_x^2 + L_y^2}\right)}{L_x\left(L_y + \sqrt{L_x^2 + L_y^2}\right)} \right] \right\}. \end{aligned} \tag{30}$$

Ekman [10]:

$$L_{\mathrm{E}} = \frac{\mu_0 L_x}{6\pi} \left[3\ln\left(\frac{L_x}{L_y} + \sqrt{\frac{L_x^2}{L_y^2} + 1} \right) + \frac{L_x^2}{L_y^2} + \frac{L_y}{L_x} + 3\frac{L_x}{L_y} \ln\left(\frac{L_y}{L_x} + \sqrt{1 + \frac{L_y^2}{L_x^2}} \right) - \left[\left(\frac{L_x}{L_y} \right)^{4/3} + \left(\frac{L_y}{L_x} \right)^{2/3} \right]^{3/2} \right]. \tag{31}$$

Asymptotic values for large aspect ratios

The asymptotic expressions for large aspect ratios, i.e. when $L_x/L_y \to \infty$, used in the comparison with the present formulation are derived from the expression in [8–11] and listed below.

$$R_{\mathrm{B},\infty} = 1.665 \frac{2L_x}{\sigma L_y L_z}. \tag{32}$$

$$R_{\mathrm{S},\infty} = \frac{4L_x}{\sigma L_y L_z}. \tag{33}$$

$$R_{E,\infty} = R_E \tag{34}$$

$$L_{\mathrm{B},\infty} = 1.665 \frac{2\mu_0 L_x}{9} \tag{35}$$

$$L_{\mathrm{S},\infty} = \frac{2\mu_0 L_x}{3\pi} (1 + 2\ln 2) \tag{36}$$

$$L_{E,\infty} = \frac{\mu_0 L_x}{2\pi} \ln\left(\frac{2L_x}{L_y} \right) \tag{37}$$

References

1. J. Li, G. Yang, Equivalent subdomain method for performance prediction of permanent magnet eddy current brakes. IET Electr. Power Appl. **15**, 1174–1186 (2021). https://doi.org/10.1049/elp2.12087
2. F. Cortés, O. Zarraga, I. Sarría, M.J. Elejabarrieta, Eddy currents damping understood as Zener viscoelastic damping. J. Sound Vib. **547**, 117539 (2023). https://doi.org/10.1016/j.jsv.2022.117539
3. F. Ye, X. Ren, G. Liao, T. Xiong, J. Xu, Mathematical model and experimental investigation for eddy current separation of nonferrous metals. Results Phys. **17**, 103170 (2020). https://doi.org/10.1016/j.rinp.2020.103170
4. H. Menana, M. Féliachi, Modeling the response of a rotating eddy current sensor for the characterization of carbon fiber reinforced composites. Eur. Phys. J. Appl. Phys. **52**, 23304 (2010). https://doi.org/10.1051/epjap/2010079
5. Belahcen A, Kouhia R, Fonteyn K. THE DIFFERENT LEVELS OF MAGNETO-MECHANICAL COUPLING IN ENERGY CONVERSION MACHINES AND DEVICES. In: Papadrakakis M, Onate E, Schrefler B, editors. Aalto Univ., 2011, p. 472–83.
6. S. Wang, X. Zhao, Y. Xia, J. Xiu, Mechanical-electromagnetic coupling elastic vibration instability of symmetrical three-phase external rotor induction motor. Nonlinear Dyn. **97**, 1–20 (2019). https://doi.org/10.1007/s11071-019-04901-1
7. R. Touzani, J. Rappaz, *Mathematical Models for Eddy Currents and Magnetostatics: With Selected Applications* (Springer, Dordrecht Heidelberg New York London, 2014). https://doi.org/10.1007/978-94-007-0202-8
8. Bialek JM, Weissenburger DW. The coupling of mechanical dynamics and induced currents in a cantilever beam. Princeton, New Jersey: Princeton Plasma Physics Laboratory; 1985.
9. N.J. Siakavellas, Analytical modelling of eddy currents induced by a time-varying magnetic field in a conductive plate. COMPEL Int. J. Comput. Math. Electr. Electron. Eng. **13**, 497–508 (1994). https://doi.org/10.1108/eb010131

10. Ekman J. Experimental verification of PEEC based electric field simulations. 2001 IEEE EMC Int. Symp. Symp. Rec. Int. Symp. Electromagn. Compat. Cat No01CH37161, Montreal, Que., Canada: IEEE; 2001, p. 351–5. https://doi.org/10.1109/ISEMC.2001.950658.
11. Ekman J, Anttu P. Parallel Implementations of the PEEC Method. 2007 IEEE Int. Symp. Electromagn. Compat., Honolulu, HI, USA: IEEE; 2007, p. 1–6. https://doi.org/10.1109/ISEMC.2007.192.
12. B.M. Notaroš, *Electromagnetics*, International edition. (Pearson, Upper Saddle River, NJ, 2011)
13. M. Brun, F. Cortés, M.J. Elejabarrieta, A methodology for analysing the influence of design variables in beams with eddy current damping. Mech. Syst. Signal Process. **234**, 112790 (2025). https://doi.org/10.1016/j.ymssp.2025.112790
14. N.J. Siakavellas, Two simple models for analytical calculation of eddy currents in thin conducting plates. IEEE Trans. Magn. **33**, 2245–2257 (1997). https://doi.org/10.1109/20.573839